Focussed on Structural Integrity and Safety: Experimental and Numerical Perspectives

Visual Abstract

Effect of different parameters controlling the flexural behavior of RC beams strengthened with NSM using nonlinear finite element analysis

Ramy Reda
Higher Technological Institute, Egypt
ramy_mostafa12000@yahoo.com, http://orcid.org/0000-0002-3298-7925

Zeinab Omar, Hossam Sallam, Seleem S. E. Ahmad
Zagazig University, Egypt
zomar73@yahoo.com, http://orcid.org/0000-0002-5531-9014
hem_sallam@yahoo.com, http://orcid.org/0000-0001-9217-9957
seleemahmad62@yahoo.com, http://orcid.org/0000-0001-9894-0209

ABSTRACT. Near surface mounted technique become the most attractive technique for strengthening RC structures. A lot of research had been conducted to study experimentally the flexural behavior of RC members strengthened with NSM technique unlike the numerical research. A numerical investigation utilizes the non-linear finite element (FE) modeling using ANSYS was performed. The developed FE model considers the behavior of the epoxy-concrete interface using cohesive zone model (CZM) which is capable of predicting the failure mode of the strengthened beams. The parametric study include the effect of different parameters such as NSM bar number, NSM bar length, end inclination angle and end inclination leg length on the flexural behavior of strengthened beams. The results showed that, The developed FE model able to predict the expected modes of failure in NSM technique, the NSM bar length was effective till 0.5 of beam span, beams strengthened with end inclined angle 45° NSM bar gives the highest improvement in load carrying capacity, this improvement was very close in case of using end inclined angle of 60° and 90°.

KEYWORDS. Finite Element Modeling; Near Surface Mounted; Debonding; End Anchorage; Inclination Angle; Flexural Strengthening.

OPEN ACCESS

Citation: Reda, R.M., Zeinab, O., Sallam, H.E.M, Seleem S. E. Ahmad, Effect of different parameters controlling the flexural behavior of RC beams strengthened with NSM using nonlinear finite element analysis, Frattura ed Integrità Strutturale, 53 (2020) 106-123

Received: 21.03.2020
Accepted: 12.04.2020
Published: 01.07.2020

INTRODUCTION

Reinforced concrete constructions are widely used over the world, after a while use it will deteriorates, demolition or rebuild will lead to bleeding the time and cost. In the last decade several techniques were conducted by many researchers to repair and strengthen the RC structures such as near surface mounted (NSM) and externally bonded

(EB) [1-7]. NSM is more effective than EB due to increasing the flexural strength for RC structures over EB by increasing bond capacity due to larger bonded surface area, furthermore it needs less installation time and makes protection against external damage by embedding the FRP bars in the concrete cover [8-10]. In NSM technique grooves are cut in the concrete cover and half of the groove filled with the adhesive, FRP bars inserted into the groove, the remaining half of the adhesive filled in the groove and leveled [7]. NSM technique has a better bond performance compared to EB, the two interfaces of NSM (concrete-adhesive, adhesive-FRP) are affected by FRP properties, FRP bar length, bar diameter, FRP bar surface treatment, groove geometry, groove size and concrete properties [11, 12]. Several investigations were performed to study the flexural behavior of RC beams strengthened with NSM FRP reinforcement. Hassan et al. [13] studied the effect of CFRP bar length, groove width and the strength of concrete on the flexural behavior of concrete structures, the results suggested that the NSM CFRP bars length should not be less than 80 times the diameter of the used bars and the resistance of concrete split failure increased by the increasing of the groove width and/or using high strength concrete.

Al-Mahmoud et al. [14] studied the effect of using two different diameter of CFRP bars; 6 and 12mm, type of concrete conventional or high-strength concrete and two types of filling materials (resin and mortar) on the flexural behavior. The results concluded that using CFRP bars with 12mm diameter increase the carrying load capacity by 83.6% compared with beams strengthened with 6mm bar diameter, on the other hand the concrete strength doesn't effect on the load carrying capacity if the failure of the strengthened beams are due to NSM system failure, also the failure mode can be changed by the type of adhesive used.

Finite element analysis either by ANSYS or ABAQUS software showed that it is a good solution in different structures problems [15-17]. Hawileh [18] developed 3D nonlinear FE ANSYS model to predict the load carrying capacity of RC beams strengthened with NSM FRP bars and validate this model by comparing the predicted results with the experimental results obtained by Al-Mahmoud et al. [14]. Then study the effect of using different types of FRP bars materials such as CFRP, AFRP and GFRP and CFRP bar diameter. The results showed very good agreement between the ANSYS model and the experimental results, all types of FRP bars enhance the flexural strength especially CFRP which increase the strength by 18.5% and 43.8% compared to AFRP and GFRP bars, respectively. Furthermore the increasing of the FRP diameter has a significantly effect on load carrying capacity of the strengthened RC beams [18].

Reda et al. [8] studied the effect of GFRP bar length on the flexural strength of RC beams, The beam strengthened with GFRP bar length 1000, 1200, 1400 and 1800mm, and also studied different epoxy length effect and end anchorage using GFRP bars with bent end inclined by 45º and 90º and others straight on the flexural strength of RC beams. The author concluded that the beam strengthened with GFRP bars of length 1400mm gives the higher load carrying capacity, the results showed that either the beams strengthened with bent end GFRP bars inclined by 45º showed superior flexural behavior over the beams strengthened with bent end GFRP bars inclined by 90º or straight bars. On the other hand a little effect of partial bonded in the constant moment region on the flexural behavior of strengthened beam. EL-Emam et al. [19] studied experimentally and numerically the effect of NSM GFRP bars length, area of main steel reinforcement and the thickness of the concrete cover on the flexural response of strengthened RC beams, the author used different GFRP bars length; 550, 1150 and 1800mm, also used 30mm and 50mm concrete cover. The results showed that increasing of GFRP bar length increase the flexural strength, the same observation when increasing the main steel reinforcement ratio from 2-Ø10mm to 2-Ø16mm the ultimate load will be increased, the opposite observation when increasing the concrete cover thickness the flexural capacity will be decreased, the numerical results showed a good agreement with the experimental results [19].

Sharaky et al. [20] studied the effect of NSM strengthening location, NSM strengthening pattern, NSM FRP strips number and of the groove depth on the flexural behavior strengthened RC beams. Two different location of NSM strengthening, near the bottom surface of the beams and beneath the stirrups, the results showed that a significantly enhancement on the ultimate load of the strengthened beams in case of installing the NSM strengthening beneath the stirrups compared with installing the NSM strengthening near the bottom surface of the beam, furthermore using two NSM FRP strips installed in one slot beneath the stirrups increase the load carrying capacity by 187% if compared with control beam. Also the groove depth gives a noticeable effect.

Although a lot of research had been carried out to study the flexural behavior of RC members strengthened with NSM technique experimentally, further numerical researches are still required to understand the effect of several parameters on the flexural behavior of RC members. In this paper the effect of many parameters such as NSM bar number, NSM bar length, end inclination angle and end inclination leg length on the flexural behavior of strengthened beams with NSM technique were studied numerically using non-linear finite element FE modeling. The numerical FE model was compared with experimental results conducted from another research [8].

FINITE ELEMENT FE MODEL

Non-linear finite element FE using (ANSYS -Version 19.0) was performed to study the flexural behavior of RC beams strengthened with NSM technique [21]. First the present model was verified by comparing the model with the experimental results conducted by Reda et al. [8]. After validation, a parametric study was conducted.

Elements Description

ANSYS element library includes several elements which can be used to simulate the different types of materials [21]. In this research (SOLID65) was used to simulate concrete and epoxy adhesive, (SOLID65) has eight nodes with three degrees of freedom at each node – translations in the nodal x, y, and z directions. SOLID65 has the ability to crack in tension and crush in compression. The Willam and Warnke criterion was used to define the failure of concrete [15, 22], it is the available model in ANSYS material library to model concrete [15]. A (LINK180) element was used to model the steel reinforcement and NSM FRP bars. Two nodes are required for this element. Each node has three degrees of freedom, – translations in the nodal x, y, and z directions. The element is also capable of plastic deformation. An eight-node solid element (SOLID45) was used for the steel plates (Loading or supports) in the models. The element is defined with eight nodes having three degrees of freedom at each node-translations in the nodal x, y, and z directions [21].

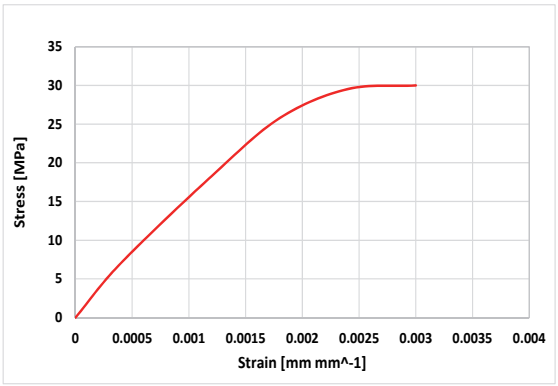

(a) Concrete in compression

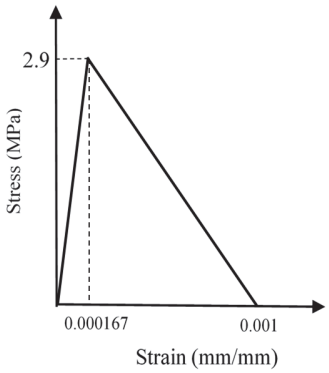

(b) Concrete in tension [22]

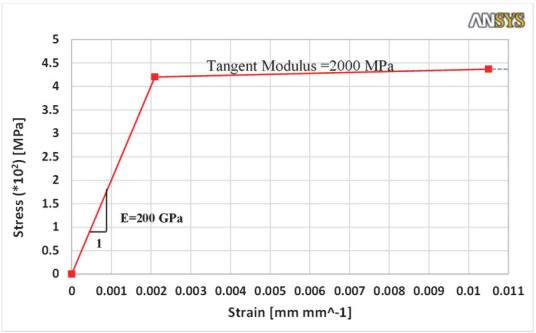

(c) Steel

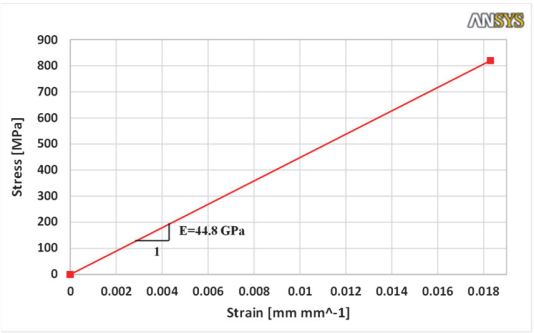

(d) GFRP

Figure 1: The stress strain curves used in model; concrete, steel and GFRP.

Materials Modeling

Concrete, steel and GFRP stress strain curves used in model are shown in (Fig.1). (Fig. 1-a) defined the concrete as a material with a nonlinear behavior with a compressive strength, tensile strength, elastic modulus and Poisson's ratio of 30 MPa and 2.9 MPa, 20 GPa and 0.2 respectively, open and closed crack shear coefficients were taken as 0.4 and 0.8 respectively, (ε_0 is the strain at the ultimate compressive strength = $2f_c'/E_c$ and; E_c is the concrete elastic modulus [23]). (Fig. 1-d) shows the concrete behavior in tension simulated by smeared crack approach. Smeared crack approach has been adopted to define the concrete behavior in tension. The smeared crack approach was discussed previously by the authors [24]. The steel reinforcement was assumed to have an elastic-perfectly plastic response, (Fig. 1-c) shows the elastic-strain hardening behavior for the reinforcing steel bars with yield stress, elastic modulus and Poisson's ratio of 420 MPa, 200 GPa and 0.3 respectively. The NSM GFRP bars were considered to be linear elastic up to failure, (Fig. 1-d), with tensile strength, elastic

modulus and Poisson's ratio of 820 MPa, 44.8 GPa and 0.26 respectively. The material used to model concrete was also used to define the adhesive behavior with tensile strength, elastic modulus and Poisson's ratio of 24.8 MPa, 4.48 GPa and 0.37 respectively. While the steel plates (loading or supports) were modeled as rigid elastic material having a modulus of elasticity and Poisson's ratio of 200 GPa and 0.3 respectively.

Concrete-Epoxy Interface

The epoxy-concrete interface was defined by two element types (CONTA174 and TARGE170) which can be used for pair-based contact, element type TARGE170 was used to model the target surface (concrete), while the element type (CONTA173) was used to model the contact surface (epoxy). CONTA174 is applicable to 3-D structural and coupled-field contact analyses, the element is used to represent contact and sliding between 3-D target surfaces and a deformable surface defined by this element. On the other hand TARGE170 is capable to represent various 3D target surfaces for the associated contact elements [21, 25 and 26]. Mixed-mode debonding based on normal tension stress-gap and shear stress-slip was assigned to the contact surface by developing the CZM in ANSYS menu [25, 26]. The maximum normal contact stress (Eqn. (1) [26]) and the contact gap at the completion of debonding (Eqn. (2) [26]) used to the tension stress-gap model were 3.28 MPa and 0.045 mm respectively.

$$\sigma_{max} = 0.6\sqrt{f_c'} \quad \text{(MPa)} \tag{1}$$

$$u^c_n = G_{f0}\left(\frac{\sqrt{10}\,f_c'}{24.3}\right)^{0.2} \quad (mm) \tag{2}$$

where is the σ_{max} is the maximum normal contact stress, f_c' the concrete compressive strength, u^c_n is the contact gap at the completion of debonding and G_{f0} is the base value of fracture energy which depends on the maximum aggregate size and equal 0.03475 N/mm as reported in CEB-FIP Model Code [27].

For the shear stress-slip model, the maximum equivalent tangent contact stress and tangential slip at the completion of debonding were 6.74 MPa and 1.086 mm respectively, as calculated Using Eqs. (3)-(5) [26].

$$\tau_{max} = (0.802 + 0.078\,\varphi)\,f_c'^{0.6} \quad \text{(MPa)} \tag{3}$$

$$u^c_t = \frac{0.976\varphi^{0.526}}{0.802 + 0.078\varphi} \quad (mm) \tag{4}$$

$$\varphi = \frac{\text{Groove depth} + 1\text{ mm}}{\text{Groove width} + 2\text{ mm}} \quad \text{(mm/mm)} \tag{5}$$

where τ_{max} is the maximum shear contact stress, φ the aspect ratio of the interface failure plane, f_c' the concrete compressive strength, and u^c_t the contact slip at the completion of debonding [26].

Model Geometry

The same geometry, dimensions, material properties and boundary conditions for all simulated beams. Concrete beam, boundary conditions and meshing of the FE model for CB, beam 2G-0.8/S and beam 2G-0.5-60/100 as an example were shown in (Fig. 2). Furthermore two rigid steel supports and loading plates were also modeled to transfer the applied loads and reduce the stress concentration if the loads are applied directly to the concrete elements. Sensitivity analysis was performed by studying the effect of element size 15, 20, 25 and 30 mm on the results of the numerical model for CB compared to the experimental results [8] as shown in (Fig. 3), from the comparisons the mesh element size 20 mm was more suitable to use to model all beams, and was used for all elements; concrete, steel, NSM bars, adhesive (epoxy) and steel plates (loading and supports).

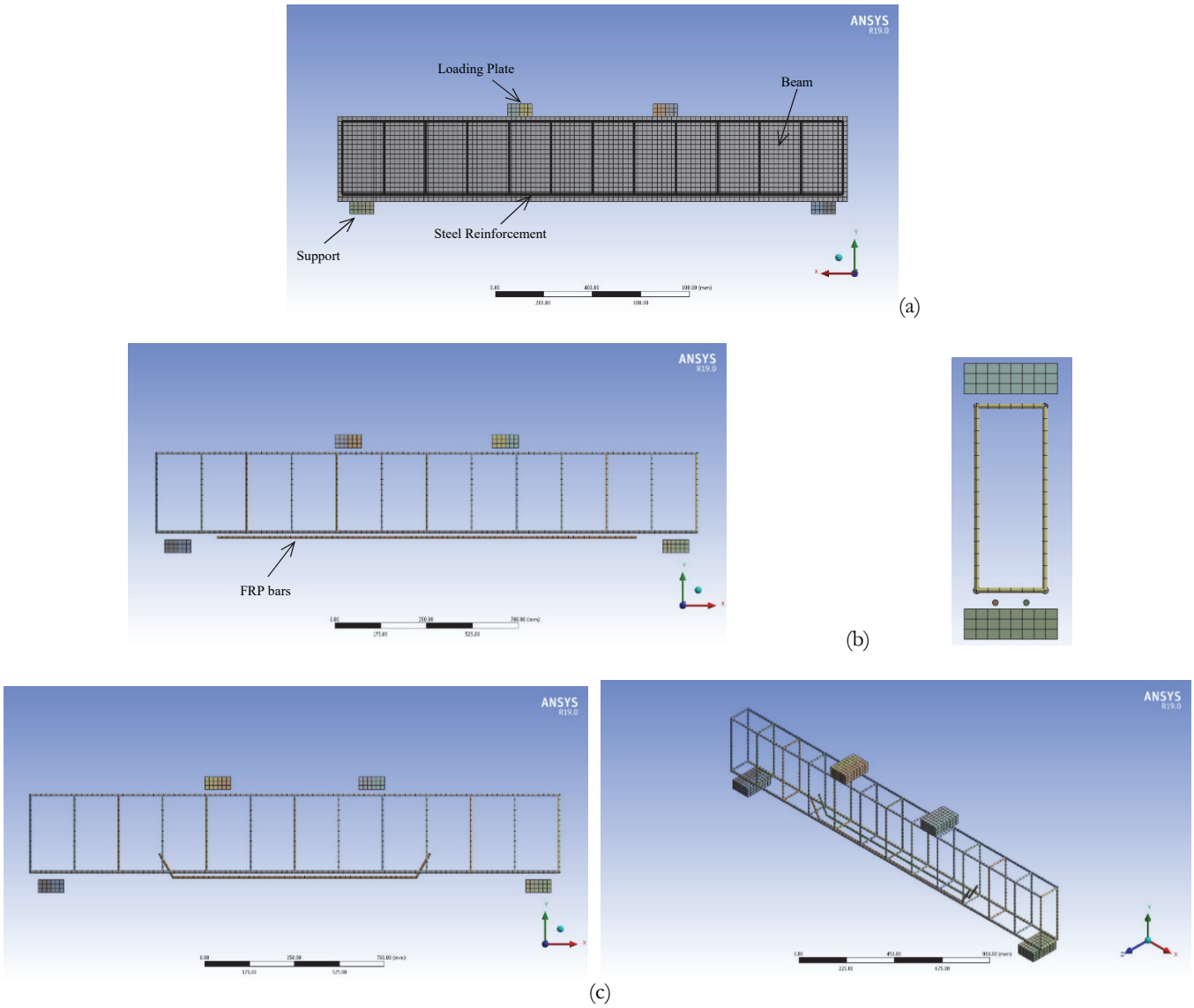

Figure 2: The simulated beams: (a) CB beam, (b) generated mesh for 2G-0.8/S beam and its cross section, (c) generated mesh for 2G-0.5-60/100 beam.

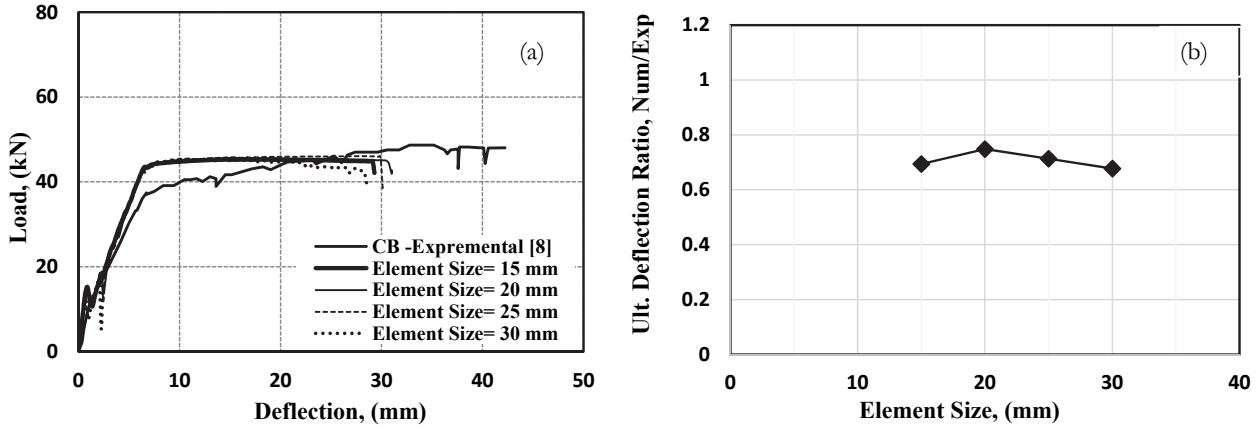

Figure 3: The effect of element size on the sensitivity of the CB model: (a) Load deflection curve, (b) Maximum deflection.

Parametric Study

The Non-linear finite element models were extended to investigate the effect of various parameters on the flexural behavior of NSM FRP strengthened beams such as; NSM bar numbers, NSM bar length, end anchorage inclination angle and end anchorage inclination length. All beams had a total length of 2200mm and a rectangular cross-section having a width of 150mm and depth of 350mm. The beams reinforcement consisted of two 12mm diameter bars for bottom reinforcement and two 10mm diameter bars for top reinforcement. As well as 8mm diameter steel stirrups were placed at a distance of 200mm. The beam details; full dimensions, reinforcement arrangements, the loading configuration and the groove locations of the modified beams were shown in (Fig. 4). The modified beams consists of one un-strengthened beam (control beam CB), and 63 strengthened beams. All beams were tested under two point loading flexural tests. The FE models were conducted to investigate the effect of various parameters on the flexural behavior of the NSM strengthened beams. Full details of the parametric study of the models are listed in (Fig. 5), Tab. 1 and explained below.

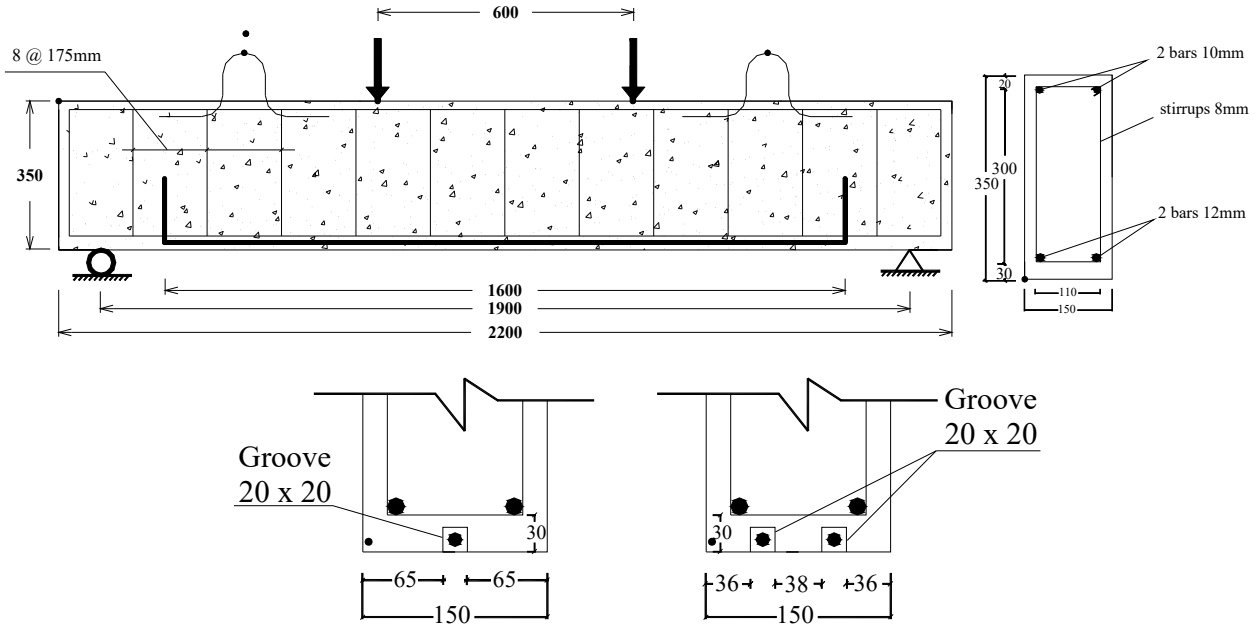

Figure 4: Beam details and grooves locations.

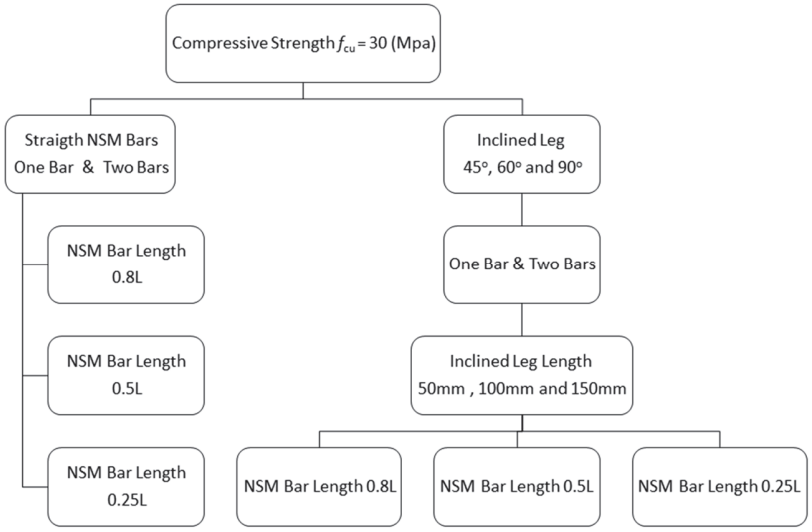

Figure 5: Full details of the parametric study of the models.

The strengthened beams were divided into four groups according to end anchorage inclination angle; S (straight without inclined leg), 45°, 60° and 90°. The first group contains six beams, the first beam was strengthened with one straight NSM bar of length 1600mm, the second beam was strengthened with one straight NSM bar of length 1000mm and the third beam was strengthened with one straight NSM bar of length 500mm. The remaining three beams are similar to the above beams but with two straight NSM bars. The three remaining groups having inclined leg, each group divided to subgroups according to the inclined leg length (50, 100 and 150mm). Second group consisted of eighteen beam divided into three subgroups as mention. **First subgroup** contain six beams, the first beam was strengthened with one NSM bar of length 1600mm with end inclined angle 45° and end inclined leg 50mm in length, the second beam was strengthened with one NSM bar of length 1000mm with end inclined angle 45° and end inclined leg 50mm in length, the third beam was strengthened with one NSM bar of length 500mm with end inclined angle 45° and end inclined leg 50mm in length, the remaining three beams with the same details but with two NSM bars. **Second subgroup** contain six beams with the same configuration of the first subgroup but with end anchorage inclination leg length of 100mm. **Third subgroup** contain six beams with the same configuration with end anchorage inclination leg length of 150mm. The third and fourth groups with end anchorage inclination angle of 60° and 90° respectively. Tab. 1 summarizes the configuration of the modified beams. The identifications are as follows: **NG-L-I/Y** where N is refers to no of NSM bars, G = GFRP NSM bars, L = length of NSM GFRP bar (0.8 =1600 mm, 0.5 =1000 mm and 0.25 =500 mm), I is the inclination angle of the end anchorage (S = no leg, 45°, 60° and 90°) and Y is refers to end anchorage inclination length; 50, 100 and 150mm.

VALIDATION OF THE FE MODELS

A comparison between the modified model and experimental results; load deflection curve and mode of failure produced by Reda et al. [8] for the control beam (CB) and (F2-180/90) beam are shown in (Fig. 6). The comparison showed a good agreement between the developed models and experimental results at all stages of loading and in mode of failure.

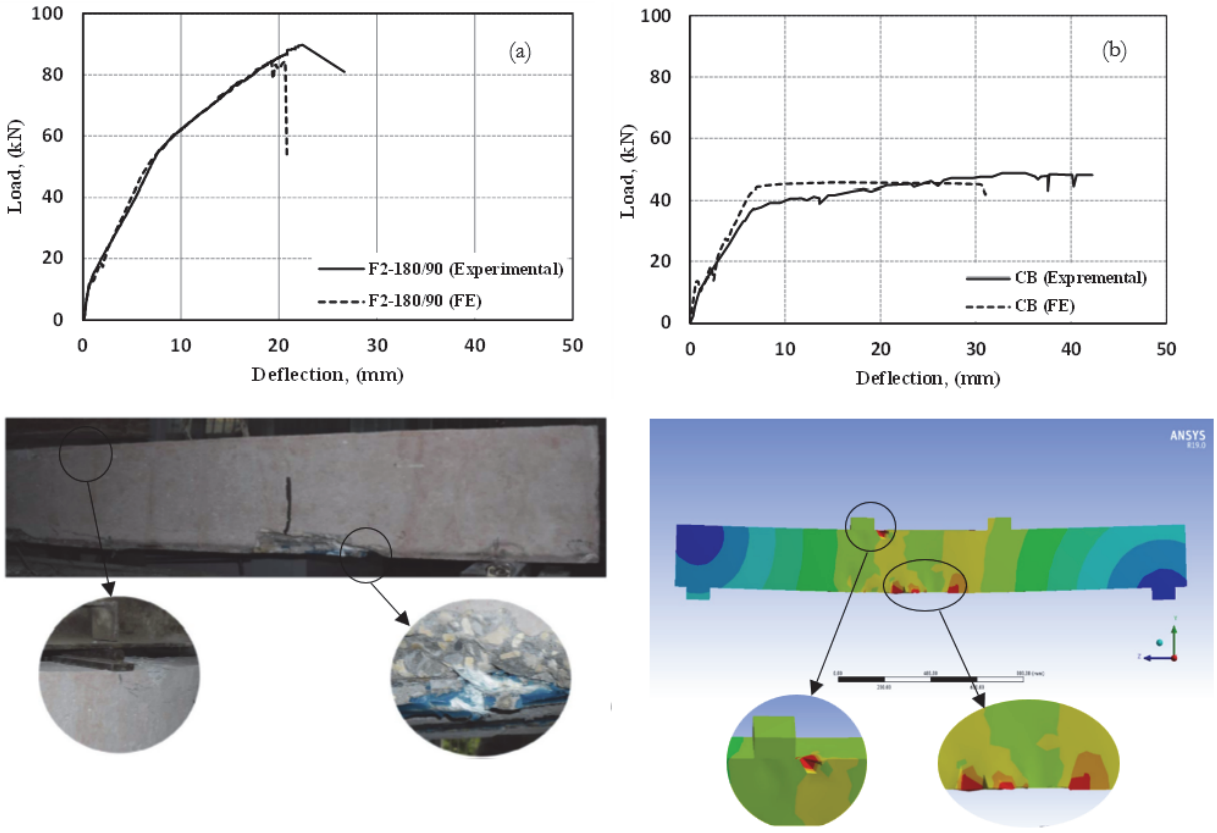

Figure 6: Comparison between experimental results presented in [8] and FE model: (a) load–deflection curve for CB, (b) load–deflection curve of beam F2-180/90 and (c) failure mode of beam 2F-180/90 and the predicted from FE.

Beam ID	N_b (-)	NSM bar length (mm)	End anchorage inclination angle	End anchorage length (mm)	Test variables
CB	-	-	-	-	Reference Beam
1G-0.8-S		1600			NSM strengthening
1G-0.5-S	1	1000	Straight	-	NSM strengthening and NSM bar length
1G-0.25-S		500			NSM strengthening and NSM bar length
2G-0.8-S		1600			NSM strengthening and NSM bar number
2G-0.5-S	2	1000	Straight	-	NSM strengthening, NSM bar length and bars no;
2G-0.25-S		500			NSM strengthening, NSM bar length and bars no;
1G-0.8-45/50		1600			End anchorage
1G-0.5-45/50		1000		50	End anchorage and bar length
1G-0.25-45/50		500			End anchorage and bar length
1G-0.8-45/100		1600			End anchorage and leg length
1G-0.5-45/100	1	1000	45	100	End anchorage, bar length and leg length
1G-0.25-45/100		500			End anchorage, bar length and leg length
1G-0.8-45/150		1600			End anchorage and leg length
1G-0.5-45/150		1000		150	End anchorage, bar length and leg length
1G-0.25-45/150		500			End anchorage, bar length and leg length
2G-0.8-45/50		1600			End anchorage and bars no;
2G-0.5-45/50		1000		50	End anchorage, bars no; and bar length
2G-0.25-45/50		500			End anchorage, bars no; and bar length
2G-0.8-45/100		1600			End anchorage, bars no; and leg length
2G-0.5-45/100	2	1000	45	100	End anchorage, bars no;, bar length and leg length
2G-0.25-45/100		500			End anchorage, bars no;, bar length and leg length
2G-0.8-45/150		1600			End anchorage, bars no; and leg length
2G-0.5-45/150		1000		150	End anchorage, bars no;, bar length and leg length
2G-0.25-45/150		500			End anchorage, bars no;, bar length and leg length
1G-0.8-60/50		1600			Leg inclination angle
1G-0.5-60/50		1000		50	Inclination angle and bar length
1G-0.25-60/50		500			Inclination angle and bar length
1G-0.8-60/100		1600			Inclination angle and leg length
1G-0.5-60/100	1	1000	60	100	Inclination angle, bar length and leg length
1G-0.25-60/100		500			Inclination angle, bar length and leg length
1G-0.8-60/150		1600			Inclination angle and leg length
1G-0.5-60/150		1000		150	Inclination angle, bar length and leg length
1G-0.25-60/150		500			Inclination angle, bar length and leg length
2G-0.8-60/50		1600			Inclination angle and bars no;
2G-0.5-60/50		1000		50	Inclination angle, bars no; and bar length
2G-0.25-60/50		500			Inclination angle, bars no; and bar length
2G-0.8-60/100		1600			Inclination angle, bars no; and leg length
2G-0.5-60/100	2	1000	60	100	Inclination angle, bars no;, bar length and leg length
2G-0.25-60/100		500			Inclination angle, bars no;, bar length and leg length
2G-0.8-60/150		1600			Inclination angle, bars no; and leg length
2G-0.5-60/150		1000		150	Inclination angle, bars no;, bar length and leg length
2G-0.25-60/150		500			Inclination angle, bars no;, bar length and leg length
1G-0.8-90/50		1600			Leg inclination angle
1G-0.5-90/50		1000		50	Inclination angle and bar length
1G-0.25-90/50		500			Inclination angle and bar length
1G-0.8-90/100		1600			Inclination angle and leg length
1G-0.5-90/100	1	1000	90	100	Inclination angle, bar length and leg length
1G-0.25-90/100		500			Inclination angle, bar length and leg length
1G-0.8-90/150		1600			Inclination angle and leg length
1G-0.5-90/150		1000		150	Inclination angle, bar length and leg length
1G-0.25-90/150		500			Inclination angle, bar length and leg length
2G-0.8-90/50		1600			Inclination angle and bars no;
2G-0.5-90/50		1000		50	Inclination angle, bars no; and bar length
2G-0.25-90/50		500			Inclination angle, bars no; and bar length
2G-0.8-90/100		1600			Inclination angle, bars no; and leg length
2G-0.5-90/100	2	1000	90	100	Inclination angle, bars no;, bar length and leg length
2G-0.25-90/100		500			Inclination angle, bars no;, bar length and leg length
2G-0.8-90/150		1600			Inclination angle, bars no; and leg length
2G-0.5-90/150		1000		150	Inclination angle, bars no;, bar length and leg length
2G-0.25-90/150		500			Inclination angle, bars no;, bar length and leg length

Table 1: Details of the parametric study of the models.

RESULTS AND DISCUSSION

The key points of the load–deflection curves obtained from the FE analysis; such as cracking load P_{cr}, yield load P_y, yield deflection Δ_y ultimate load P_u and maximum deflection Δ_u, percentage of increase in maximum load carrying capacity for strengthened beams with respect to CB P_u%, in addition to ductility index μ (the ratio of the ultimate deflection to the deflection at yielding), stiffness E, energy absorption Ω (the area under load–deflection curve) and also failure mode of the strengthened beams were presented in Tab. 2. The control beam failed due to concrete crushing after yielding of the steel reinforcement, while beams 1G-0.25/S, 2G-0.5-45/150, 2G-0.5-60/100 and 2G-0.25-90/150 for example failed due to epoxy debonding as shown in (Fig. 7) which mean that the developed FE model is capable of predicting the epoxy-concrete interface debonding failure.

Beam ID	P_{cr} (kN)	P_y (kN)	Δ_y (mm)	P_u (kN)	Δ_u (mm)	P_u %	μ	E (kN/mm)	Ω (kN.mm)	Failure mode
CB	27.5	85	4.3	90.55	21	-	4.9	65.8	1706	CC
1G-0.8-S	33	94	4.2	122.9	14.7	35.7	3.5	65.9	1403.1	CCS
1G-0.5-S	32	92	4.2	119.7	11	32.2	2.6	65.9	953	CCS
1G-0.25-S	28	91	4.5	94.7	30	4.6	6.7	66.0	2636.4	EED-CCS
2G-0.8-S	32	106	4.5	154.1	13.6	70.2	3.0	66.1	1492.4	EC
2G-0.5-S	33	105	4.6	129.9	10.1	43.5	2.2	66.2	941.9	EED
2G-0.25-S	35.5	90	4.2	96.4	19.4	6.5	4.6	66.2	1664	CCS
1G-0.8-45/50	31	93	3.6	153.6	23.15	69.6	6.4	70.8	2796.8	CC
1G-0.5-45/50	29	102	4.3	143.14	16.189	58.1	3.8	69.0	1797.7	CCS
1G-0.25-45/50	29	103	4.6	128.58	17.17	42.0	3.7	68.9	1790.5	EED
1G-0.8-45/100	29	98	0.4	145.6	18.8	60.8	47.0	68.9	2158.1	CCS
1G-0.5-45/100	29	105	4.65	147.7	28.2	63.1	6.1	68.9	3517.2	CC
1G-0.25-45/100	29	101	4.4	130.3	17.7	43.9	4.0	68.8	1864.4	CCS-EC
1G-0.8-45/150	29	99	4.1	150.5	20.9	66.2	5.1	68.9	2474.2	EC
1G-0.5-45/150	29	99	4.1	150.8	28.5	66.5	7.0	68.7	3606.5	CC
1G-0.25-45/150	29	103	4.6	139.1	24.01	53.6	5.2	68.9	2724.2	EED
2G-0.8-45/50	33	104	4	180.8	24.11	99.7	6.0	70.3	3440.1	CCS
2G-0.5-45/50	31	104	4.1	172.15	18.37	90.1	4.5	70.1	2393.9	CCS
2G-0.25-45/50	36	103	4.2	152	29.3	67.9	7.0	70.1	3664.9	EC
2G-0.8-45/100	31	117	4.9	178.28	24.8	96.9	5.1	70.1	3563.1	CC
2G-0.5-45/100	31	101	3.7	162.5	12.5	79.5	3.4	70.1	1428.7	CCS
2G-0.25-45/100	31	103	4.3	141.1	19.7	55.8	4.6	71.5	2241.2	CC
2G-0.8-45/150	34	101	4	176.2	27.2	94.6	6.8	68.8	3801.5	CC
2G-0.5-45/150	31	105	4.1	166.9	14	84.3	3.4	70.1	1688.9	EED
2G-0.25-45/150	31	100	3.9	146.9	18.3	62.2	4.7	70.0	2105.2	EC
1G-0.8-60/50	31	101	4.4	150.9	23.2	66.6	5.3	70.1	2817.6	CC
1G-0.5-60/50	30	104	4.6	150.6	23.4	66.3	5.1	70.0	2837	CCS
1G-0.25-60/50	37	103	4.8	139.5	33.2	54.1	6.9	70.4	3966.5	EED
1G-0.8-60/100	29	107	4.8	159.8	33.4	76.5	7.0	70.2	4403.5	IED
1G-0.5-60/100	29	104	4.7	160.6	33.46	77.4	7.1	69.9	4382.5	CC
1G-0.25-60/100	36	95	4	135	19.88	49.1	5.0	69.9	2152.1	CCS
1G-0.8-60/150	30	105	4.6	154.6	28.6	70.7	6.2	70.2	3661	CC
1G-0.5-60/150	30	101	4.2	146.2	20.9	61.5	5.0	70.0	2481.9	CCS
1G-0.25-60/150	33	96	4.1	136.6	22.2	50.9	5.4	70.1	2478.7	EED

2G-0.8-60/50	32	108	4	175.5	23.7	93.8	5.9	71.0	3375.9	CCS
2G-0.5-60/50	33	96	3.4	169.5	15.8	87.2	4.6	71.2	1975.7	EED
2G-0.25-60/50	31	103.8	4.4	148.1	30.6	63.6	7.0	71.1	3776.9	EED
2G-0.8-60/100	30	97	3.8	167.4	12.6	84.9	3.3	69.7	1460.4	CCS
2G-0.5-60/100	31	107	4.1	164.7	15.3	81.9	3.7	71.3	1881.1	EED
2G-0.25-60/100	31	101	3.9	142.3	19.7	57.2	5.1	70.2	2287.1	SF
2G-0.8-60/150	37	104	4.2	167.9	19.5	85.4	4.6	71.0	2593.5	CCS
2G-0.5-60/150	31	106	4	167.5	15.4	85.0	3.9	71.5	1933.9	CCS
2G-0.25-60/150	31	107	4.5	143.9	24.7	58.9	5.5	70.8	2933.4	CCS
1G-0.8-90/50	29	96	3.8	153.1	29	69.1	7.6	70.0	3646.9	CC
1G-0.5-90/50	30	100	4.4	148.6	25.2	64.1	5.7	69.9	3057.1	CC
1G-0.25-90/50	30	93	3.8	131.6	21.7	45.3	5.7	69.9	2345.8	EED
1G-0.8-90/100	29	103	4.4	152.6	35.14	68.5	8.0	69.9	4528.8	CC
1G-0.5-90/100	31	95	3.8	140.2	22.1	54.8	5.8	69.7	2576.6	EED
1G-0.25-90/100	29.5	95	4	135.2	22.1	49.3	5.5	69.7	2442.8	CC
1G-0.8-90/150	31	96	3.9	153.1	25.15	69.1	6.4	70.5	3123.8	CC
1G-0.5-90/150	30	103	4.5	145.1	20.4	60.2	4.5	69.8	2370.7	EED
1G-0.25-90/150	34	99	4.5	137.6	33.7	52.0	7.5	69.9	3970.7	EED
2G-0.8-90/50	30	106	4.2	169.8	13.3	87.5	3.2	70.2	1533.6	CC
2G-0.5-90/50	31	100.1	3.8	168.6	15.75	86.2	4.1	70.3	1932.2	CCS
2G-0.25-90/50	30	104	4.6	145.4	34	60.6	7.4	70.0	4131.2	CCS
2G-0.8-90/100	34	103	4.2	165.6	13.5	82.9	3.2	68.8	1559.9	CC
2G-0.5-90/100	33	105	4.45	156.24	14.3	72.5	3.2	68.7	1631.5	CCS
2G-0.25-90/100	35	105	4.4	141.4	31	56.2	7.0	69.6	3734	CCS
2G-0.8-90/150	33	99	3.6	168.3	16.5	85.9	4.6	70.0	2077.2	IED
2G-0.5-90/150	29	95	3.7	165	17.3	82.2	4.7	70.0	2142.8	CCS
2G-0.25-90/150	31	101	4.2	144.6	16.9	59.7	4.0	69.1	1774.8	EED

P_{cr} = load at cracking, P_y and Δ_y = load and deflection at yielding, P_u and Δ_u = load and deflection at ultimate, P_u% is the percentage increase in the load carrying capacity, μ = ductility index, E= stiffness, Ω = energy absorption (area under P-Δ curve).
CC concrete crushing, CCS concrete cover separation, EED end epoxy debonding, EC epoxy crushing, IED Intermediate epoxy debonding and SF shear failure.

Table 2: FE analysis from ANSYS results and failure modes of the beams.

Effect of NSM Bar Length

The effect of the NSM bar length on the flexural behavior of strengthened beams was investigated in this section. (Fig. 9) shows load deflection curves, mid-span steel strain and mid span FRP bars strain for different beams, the bars length were 0.8, 0.5 and 0.25 of the beam span; 1600, 1000, and 500 mm.

It is clear from (Fig. 9-a) that increasing of the NSM bar length played a significant effect in increasing the ultimate load carrying capacity, similar result was reported in [8, 19 and 25]. The load carrying capacity for beams 2G-0.8-150/90, 2G-0.5-150/90 and 2G-0.25-150/90 were 168.3, 165 and 130.9kN with increasing of 85.9, 82.2 and 44.6% respectively if compared with CB. A small noticeable enhancement in load carrying capacity between beams strengthened with NSM bar length 0.8L and 0.5L which was 2%, this may be due to the covering of the constant moment region with the bar length of 0.5L unlike the beam strengthened with FRP bar of length 0.8L which extended outside the constant moment region which lead to a little effect in increasing the load carrying capacity over beam strengthened with 0.5L bar length. The same observation in the NSM FRP load strain curve see (Fig. 9-c).

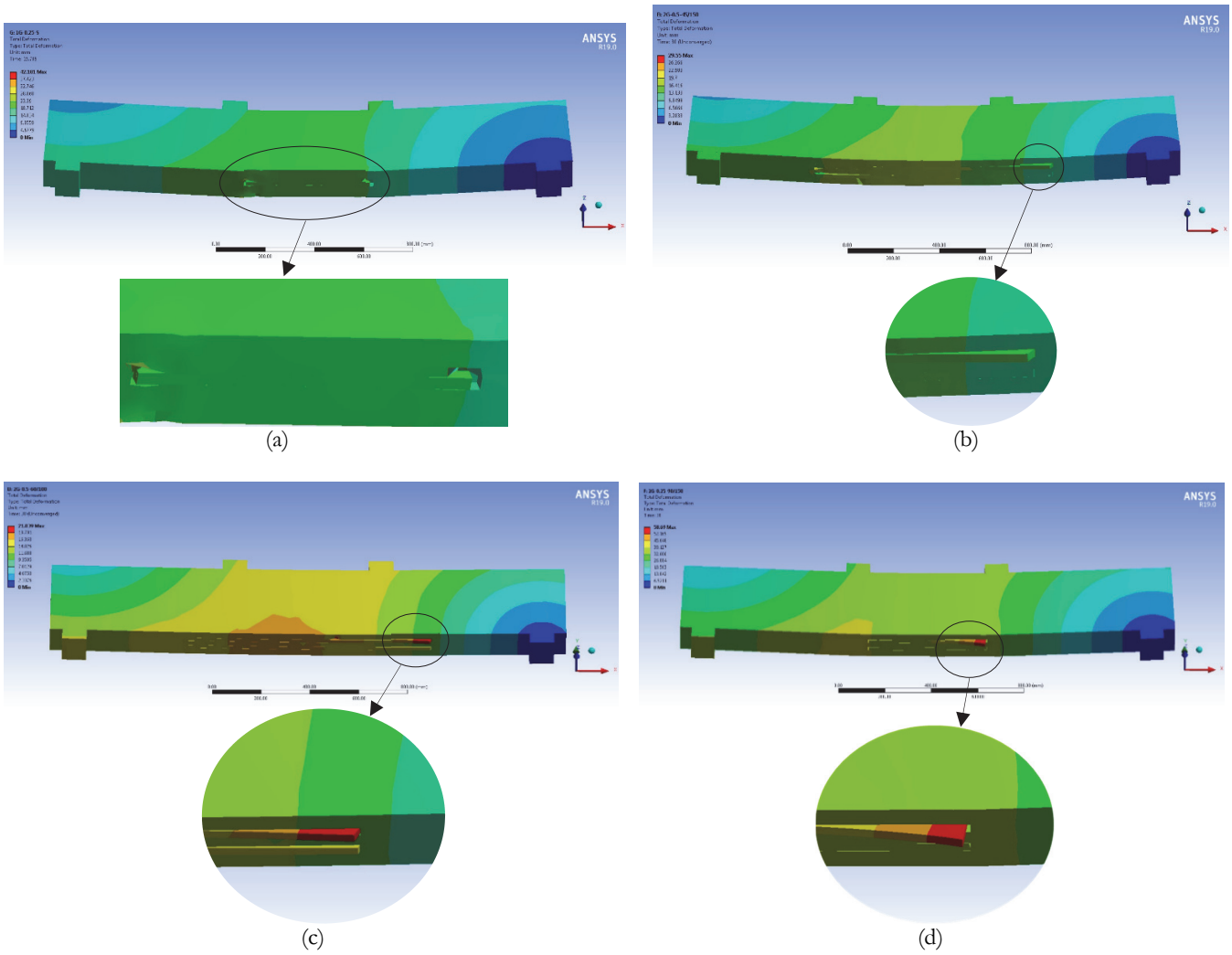

Figure 7: Failure modes of the beams: (a) 1G-0.25/S, (b) 2G-0.5-45/150, (c) 2G-0.5-60/100 and (d) 2G-0.25-90/150.

(Fig. 8) shows the predicted crack patterns from the FE analysis at failure for CB and strengthened beams; 2G-0.5-S, 2G-0.25-S and 1G-0.25-S.

(Fig. 10) shows the effect of NSM bar length for the strengthened beams on load carrying capacity with respect to load carrying capacity of the corresponding beam but without end anchorage $P_u/P_{u,\,0=0}$, noticeable enhancement (and close together) in all beams strengthened with one NSM FRP bar when use NSM bar length of 0.5L and 0.8L if compared with the same beam but without end anchorage see (Fig 10-a), greater improvement in load carrying capacity when use one NSM bar of length 0.25L with respect to the same beam without end anchorage, the big improvement reflect the great effect of the end anchorage in small NSM bars length. Beam strengthened with two NSM bars shown in (Fig 10-b), the figure confirm that the efficiency of the end anchorage increase with the decrease of the NSM bar length from length 0.8L to length 0.25L, there are noticeable enhancement in load carrying capacity when use NSM bar length of 0.5L if compared with 0.8L. The load carrying capacity of beams strengthened with same NSM bar length gives close results even though they had different parameters such as end inclination angle and end inclination leg length, this mean that the bar length is the main factor controlling the increasing of load carrying capacity of strengthened beams.

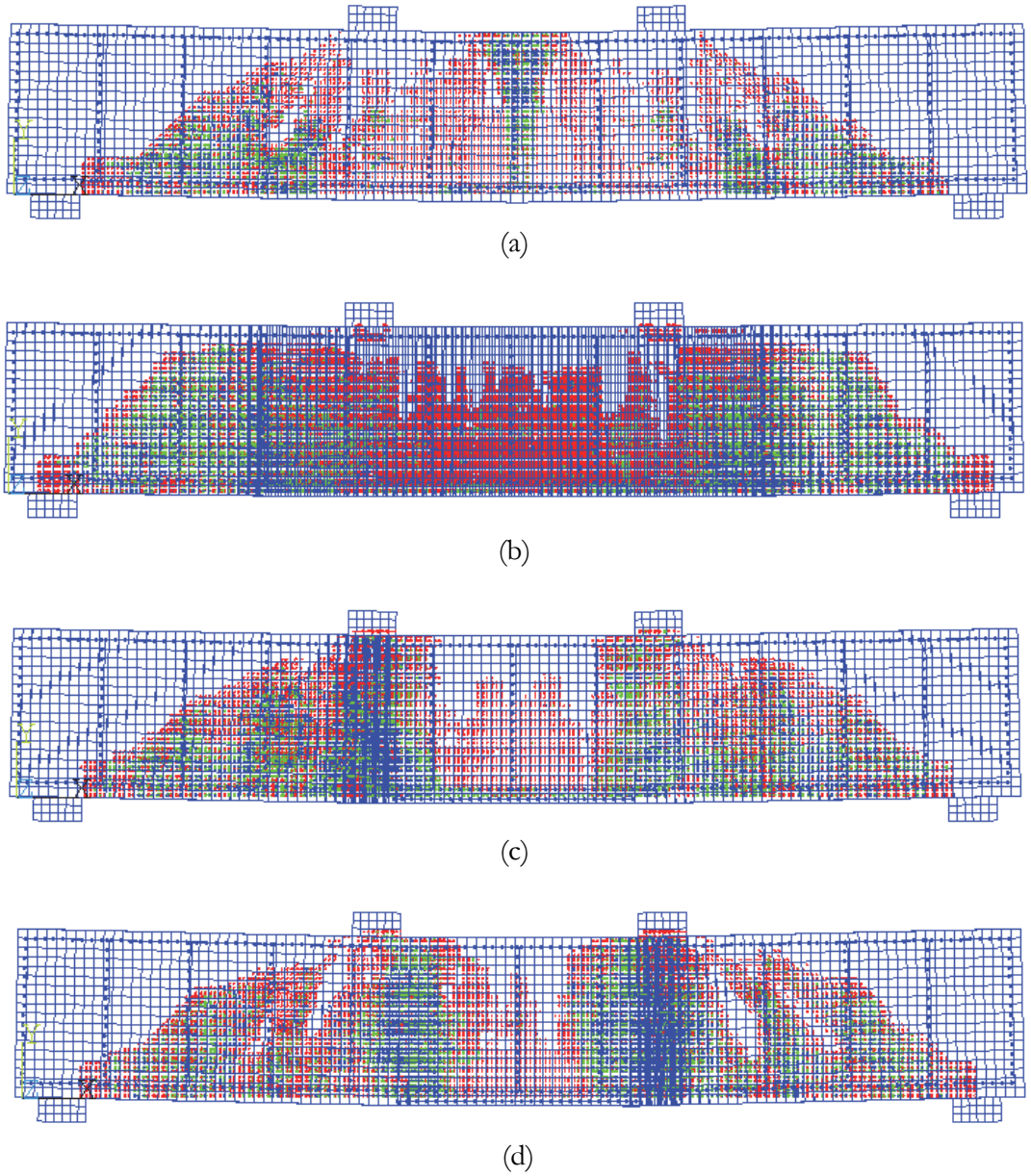

Figure 8: Predicted crack patterns of the beams at failure: (a) CB, (b) 2G-0.5-S, (c) 2G-0.25-S and (d) 1G-0.25-S.

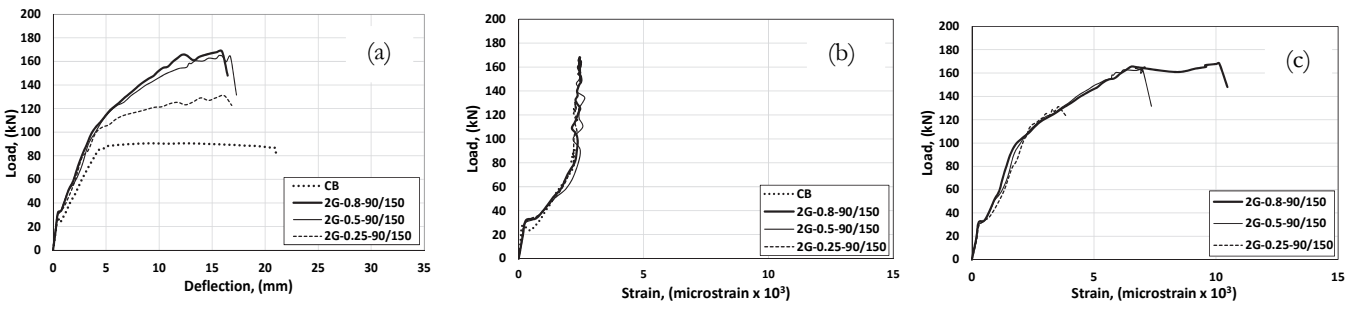

Figure 9: Effect of NSM bar length: (a) load-deflection curve, (b) steel strain and (c) FRP strain.

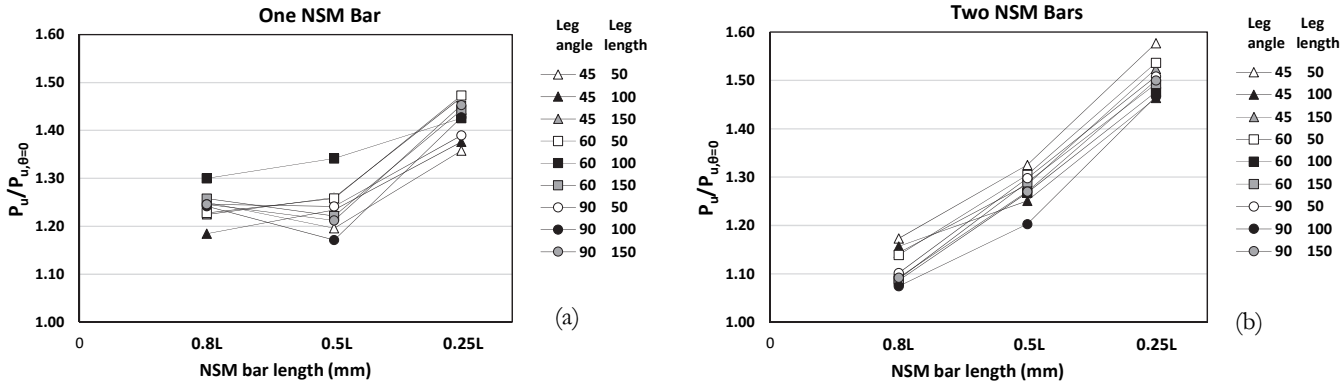

Figure 10: The effect of NSM bar length on $P_u/P_{u,\theta=0}$ for: (a) beams strengthened with one NSM bar and (b) beams strengthened with two NSM bars.

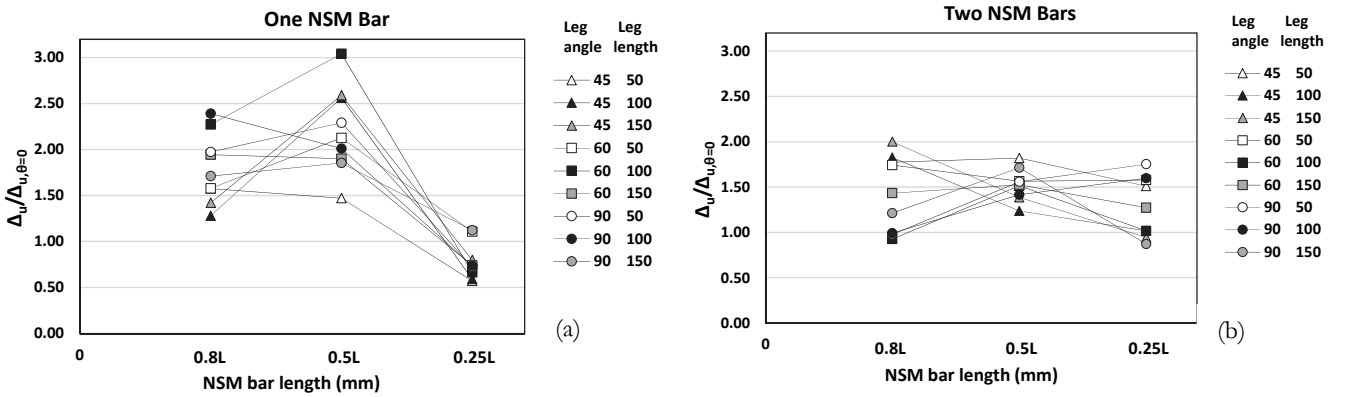

Figure 11: The effect of NSM bar length on $\Delta_u/\Delta_{u,\theta=0}$ for: (a) beams strengthened with one NSM bar and (b) beams strengthened with two NSM bars.

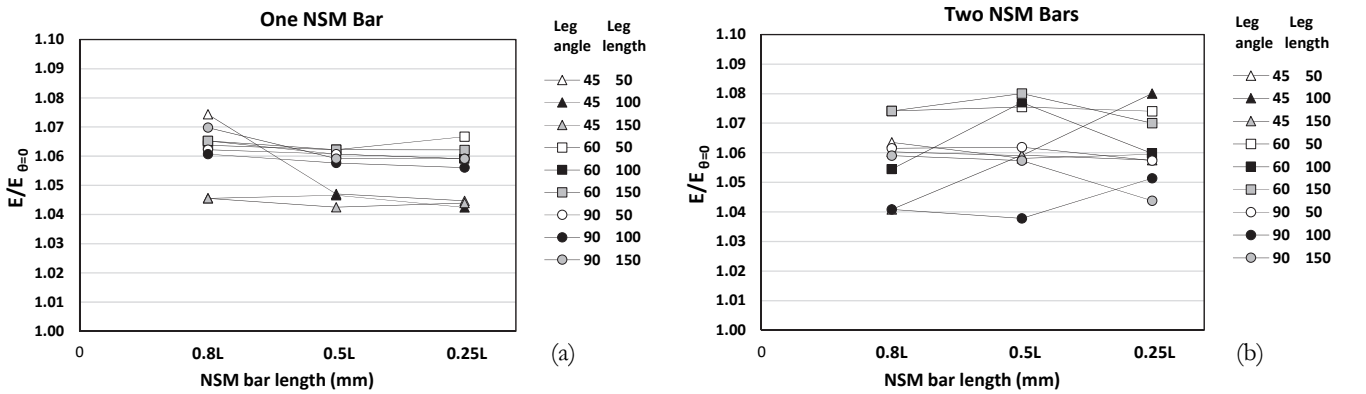

Figure 12: The effect of NSM bar length on $E/E_{\theta=0}$ for: (a) beams strengthened with one NSM bar and (b) beams strengthened with two NSM bars.

The effect of NSM bar length for the strengthened beams on maximum deflection with respect to maximum deflection of the corresponding beam but without end anchorage $\Delta_u/\Delta_{u,\theta=0}$ were shown in (Fig. 11), the highest increasing in maximum deflection were for beam strengthened with one NSM bar of length 0.5L see (Fig. 11-a). The same observation in beams strengthened with two NSM bars with end inclination angle 60° and 90° see (Fig. 11-b). (Fig. 12) shows the effect of NSM bar length on the beams stiffness compared to the stiffness of the corresponding beams but without end anchorage $E/E_{\theta=0}$, there are no noticeable changes in the stiffness of beams strengthened with one NSM bar when use different NSM bar length 0.8L, 0.5L and 0.25L see Fig (12-a).

Effect of NSM Bar Number

The effect of the NSM FRP bar number was shown in (Fig. 13), the figure clarify that the increasing of bar number in the strengthened beams from one bar to two bars increase the load carrying capacity of the strengthened beams, the load carrying capacity for beams 2G-0.5-50/90 and 1G-0.5-50/90 were 168.6 and 148.6kN with increasing of 86.2 and 64.1% respectively if compared with CB, using two bars instead of one bar increase the load carrying capacity by 13.5%, this result agree with this reported in [11], (Fig13-c) shows the same observation for the effect of NSM bar length on the strain of NSM FRP bars.

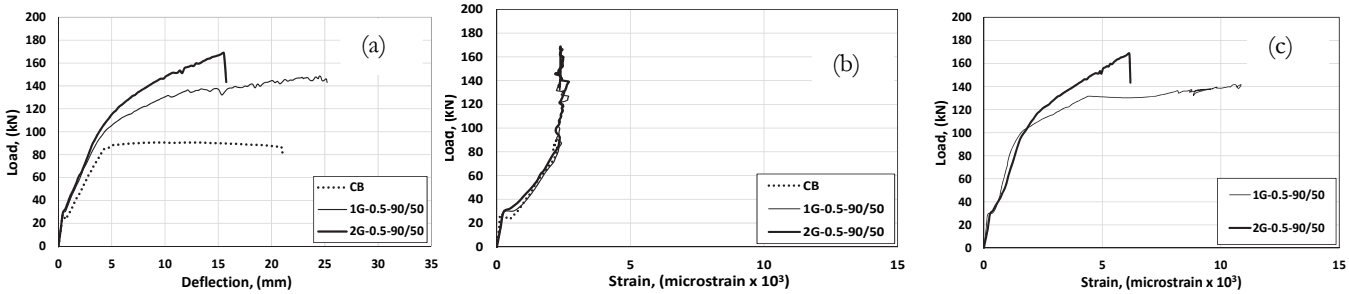

Figure 13: Effect of NSM bar number: (a) load-deflection curve, (b) steel strain and (c) FRP strain.

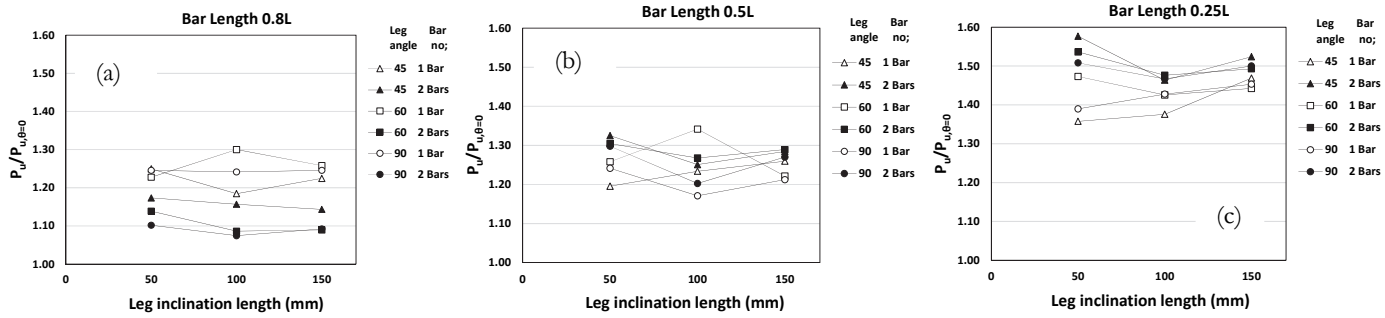

Figure 14: The effect of NSM bar number on $P_u/P_{u,\theta=0}$ for: (a) beams strengthened with bar length 0.8L, (b) beams strengthened with bar length 0.5L and (c) beams strengthened with bar length 0.25L.

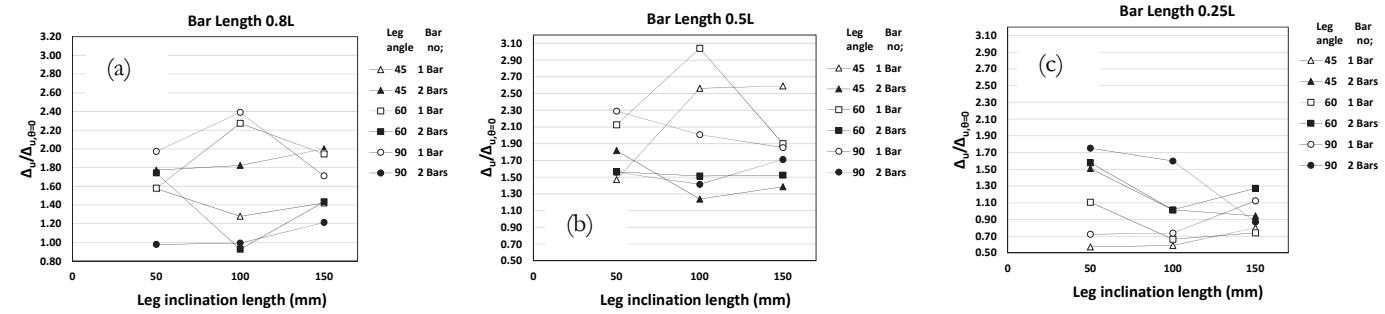

Figure 15: The effect of NSM bar number on $\Delta_u/\Delta_{u,\theta=0}$ for: (a) beams strengthened with bar length 0.8L, (b) beams strengthened with bar length 0.5L and (c) beams strengthened with bar length 0.25L.

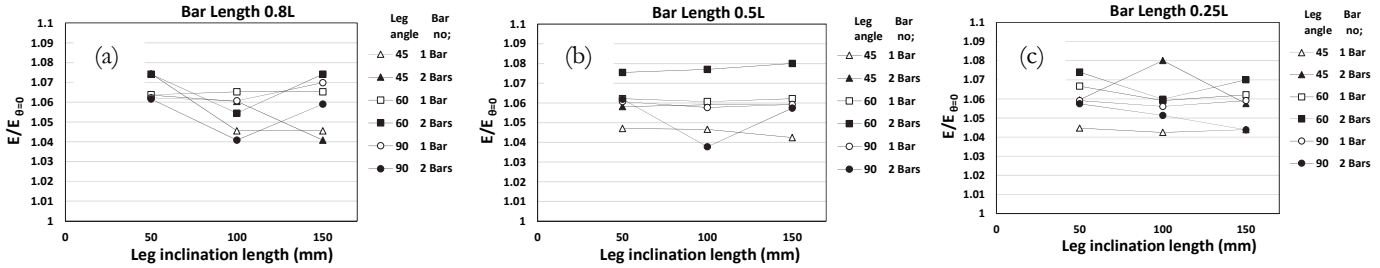

Figure 16: The effect of NSM bar number on $E/E_{\theta=0}$ for: (a) beams strengthened with bar length 0.8L, (b) beams strengthened with bar length 0.5L and (c) beams strengthened with bar length 0.25L.

The effect of the NSM FRP bar number for the strengthened beams on load carrying capacity with respect to load carrying capacity the corresponding beam but without end anchorage $P_u/P_{u,\theta=0}$ were shown in (Fig. 14), the beams strengthened with one NSM FRP bar gives higher enhancement compared to the beams strengthened with two NSM FRP bars in case of strengthening with NSM bar length of 0.8L, this may be because of the large confinement of the NSM bar compared to two bars show (Fig. 14-a). Unlike beams strengthened with two bars of length 0.5L and 0.25L gives more enhancement over beams strengthened with one NSM bar as shown in (Fig. 14-b and c), this may be due to the occurrence of the full length of the NSM bars in the maximum moment region which made it more effective, and the increasing of the bars number leads to increasing the load carrying capacity. The stiffness of the strengthened beams give the same trend of load carrying capacity see (Fig. 16).

Effect of End Anchorage Inclination Angle

In this section the effect of end anchorage inclination angle on the flexural response for CB, 2G-0.5/S, 2G-0.5-45/50, 2G-0.5-60/50 and 2G-0.5-90/50 beams are shown in (Fig. 17). In general beams strengthened with NSM FRP having end anchorage inclined by 45° gives higher load carrying capacity compared to those beams strengthened with NSM FRP having end anchorage inclined by 60°, 90° and others with straight bars that may be due to enhancement of the shear capacity of the strengthened beams, the same result was reported in [8, 24], beams strengthened with end inclination angle of 60° gives load carrying capacity close to beams strengthened with end inclination angle of 90°, as shown in (Fig. 17-a); beam 2G-0.5-45/50 with inclination angle of 45° gives the highest load carrying capacity 172.15kN which increased by 90.1% if compared with CB. The next 2G-0.5-60/50 beam with inclination angle of 60° gives 169.5kN with increase of 87.2% if compared with CB, beam 2G-0.5-90/50 with inclination angle of 90° gives 168.6kN with increase of 86.2% if compared with CB. The lower increase in load carrying capacity was in beam 2G-0.5/S with straight end which gives 129.9kN with 43.5% enhancement when compared with CB.

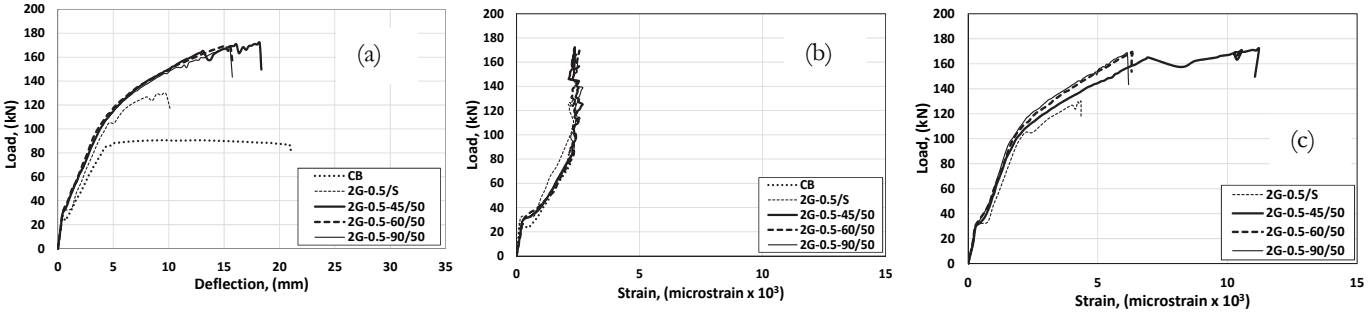

Figure 17: The effect of end anchorage inclination angle: (a) load-deflection curve, (b) steel strain and (c) FRP strain.

The effect of end anchorage inclination angle on maximum load carrying capacity P_u, maximum deflection Δ_u and stiffness E for the strengthened beams with respect to corresponding beam without end anchorage were shown in (Figs. 18, 19 and 20). From (Fig. 18) it is very clear that the beam strengthened with end anchorage inclination angle of 45° gives highest enhancement in load carrying capacity if compared with beam strengthened with end anchorage inclination angle of 60° and 90° in cases of using two NSM bars see (Fig. 18-b) and lowest enhancement in beam stiffness in beam strengthened with one NSM bar. While the large enhancement in beam stiffness in beams strengthened with two NSM bars and end anchorage inclination angle of 60° as shown in (Fig. 20-b).

Beams strengthened with end anchorage inclination angle of 90° gives the lowest load carrying capacity if compared with beams strengthened with end anchorage inclination angle of 45° and 60° as shown in (Fig.18).

Effect of End Anchorage Leg Length

The effect of the NSM FRP end anchorage leg length on the flexural behavior of beams was shown in (Figs. 18 to 21), the figures presents a comparison between different beams with the same NSM FRP bar numbers, bar length and end anchorage inclination angle, the difference was in end anchorage length 50, 100 and 150mm. As shown in the (Fig. 21) beams strengthened with end anchorage length of 50 and 150mm gives nearly the same load carrying capacity and highest than beams strengthened with end anchorage length of 100mm.

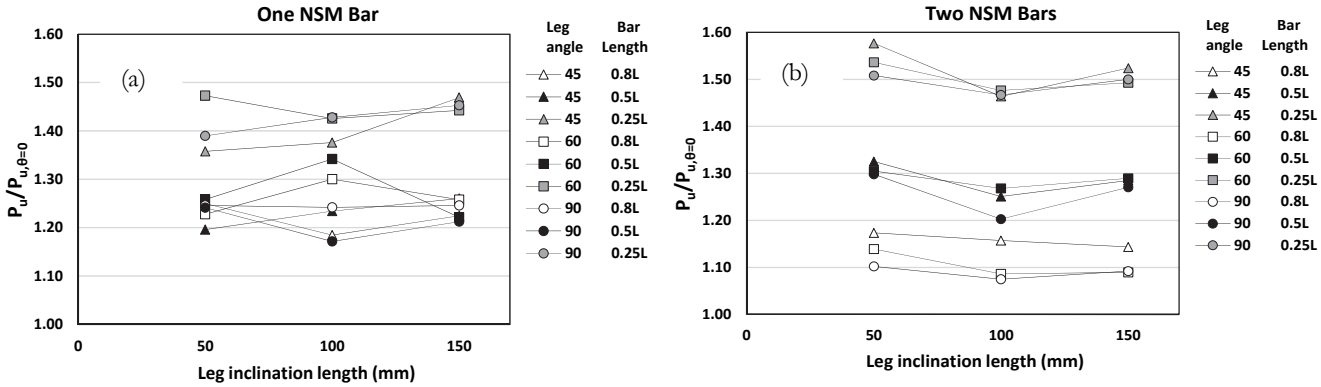

Figure 18: The effect of end anchorage inclination angle and length on $P_u/P_{u,\theta=0}$ for: (a) beams strengthened with one NSM bar and (b) beams strengthened with two NSM bars.

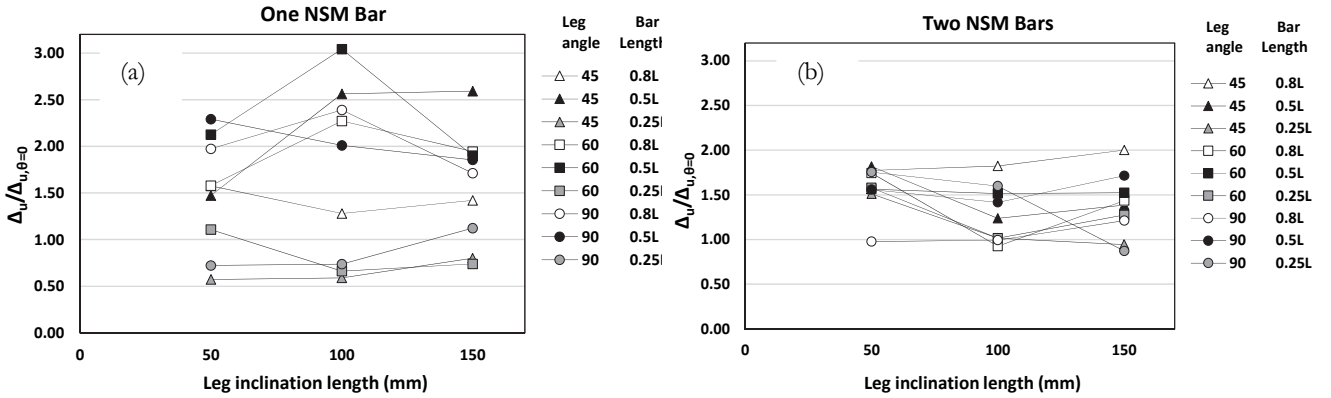

Figure 19: The effect of end anchorage inclination angle and length on $\Delta_u/\Delta_{u,\theta=0}$ for: (a) beams strengthened with one NSM bar and (b) beams strengthened with two NSM bars.

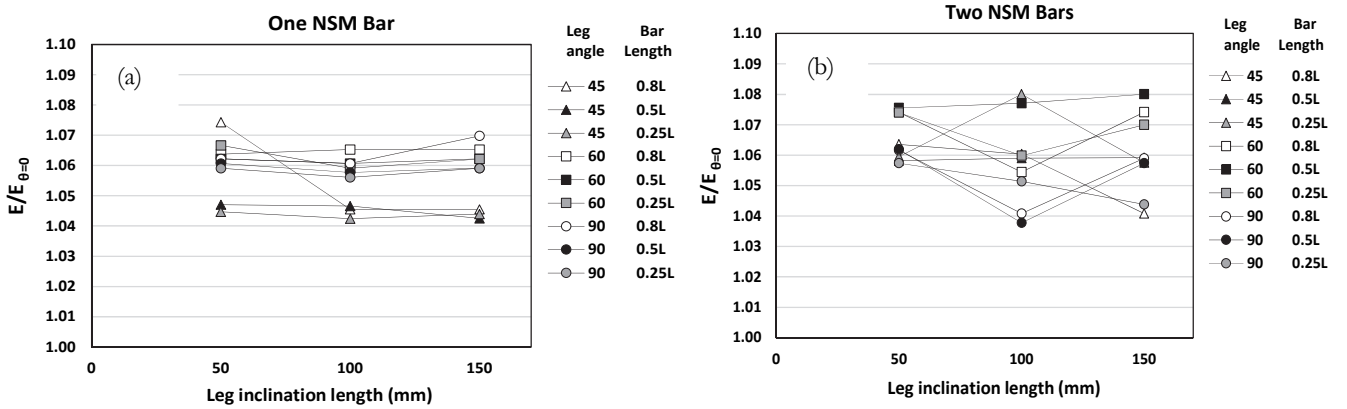

Figure 20: The effect of end anchorage inclination angle and length on $E/E_{\theta=0}$ for: (a) beams strengthened with one NSM bar and (b) beams strengthened with two NSM bars.

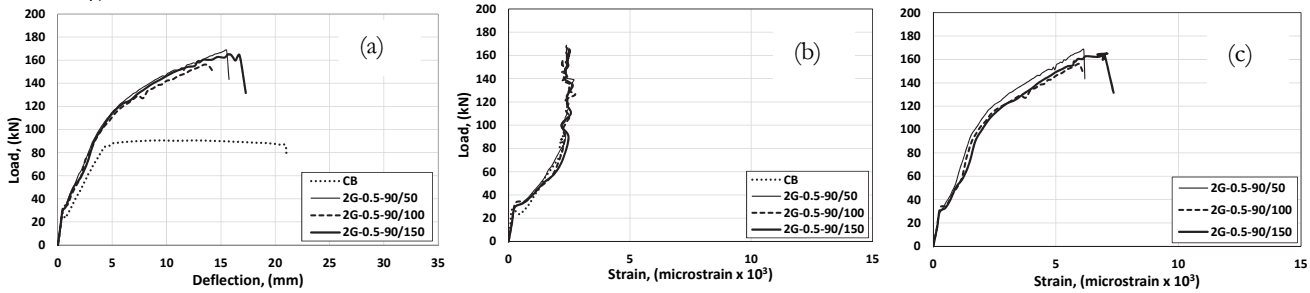

Figure 21: The effect of end anchorage length: (a) load-deflection curve, (b) steel strain and (c) FRP strain.

Beam strengthened with end inclination leg of length 0.25L gives the highest enhancement in term of load carrying capacity if compared to same beam without leg in beams strengthened with both one and two NSM FRP bars as shown in (Fig. 18-a, b).

CONCLUSIONS

Based on the results presented in this paper conducted from the developed FE model, the following conclusions can be drawn:

- The developed FE model is suitable for modeling and analyzing RC beams strengthened using NSM technique in flexure, and capable of predicting the different expected modes of failure.
- Increasing the NSM bar length up to 0.5L has a considerable effect on the load-carrying capacity of the strengthened RC beams, while a little effect if the length increased to 0.8L if compared with beams strengthened with NSM bar length 0.5L.
- In case of strengthening with NSM bar length of 0.8L, the efficiency of inclined leg is more pronounced in one bar than that in two bars i.e. (P_u for beams strengthened by NSM with leg/P_u for beams strengthened by NSM without leg) in case of one bar ranged from 1.18 to 1.30 and in case of two bars ranged from 1.07 to 1.17. A different conclusion in case of using two NSM bars with length of 0.5L and 0.25L which gives the higher enhancement, this may be due to the occurrence of the NSM bars in the maximum moment region which made it more effective, and the increasing of the bars number leads to increasing the load carrying capacity.
- The strengthened beam with end anchorage inclined angle of 45° showed superior flexural behavior in term of load carrying capacity over strengthened beam with end anchorage inclined angle of 60°, 90° and other straight.

REFERENCES

[1] Wu, Z., Wang, X. and Iwashita, K. (2007). State-of-the-Art of Advanced FRP Applications in Civil Infrastructure in Japan, Composites & Polycon, American Composites Manufacturers Association, Tampa, FL USA, pp. 1-13.

[2] Lorenzis, L.D. and Teng, J.G. (2007). Near-surface Mounted FRP Reinforcement: An Emerging Technique for Strengthening Structures, Composites Part B, 38, pp.119-143.

[3] Laraba, A., Merdas, A. and Chikh, N. (2014). Structural Performance of RC Beams Strengthened with NSM-CFRP, Proceedings of the World Congress on Engineering, II, pp. 958-966.

[4] Bilotta, A., Ceroni, F., Nigro, E. and Pecce, M. (2015). Efficiency of GFRP NSM strips and EBR plates for flexural strengthening of RC beams and loading pattern influence, Composites Structures, 124, pp. 163-175.

[5] American Concrete Institute ACI 440. (2017). Guide for the design and construction of externally bonded FRP systems for strengthening concrete structures. MI, USA: Farmington Hills; (ACI 440.2R-17).

[6] Zhang, S.S., Yu, T. and Chen, G.M. (2017). Reinforced concrete beams strengthened in flexure with near-surface mounted (NSM) CFRP strips: Current Status and Research needs, Composites Part B, 131, pp. 30-42.

[7] Zhang, S.S. (2018). Bond strength model for near-surface mounted (NSM) FRP bonded joints: Effect of concrete edge distance, Composite Structures, 201, pp. 664-675.

[8] Reda, R.M., Sharaky, I.A., Ghanem, M., Seleem, M.H. and Sallam, H.E.M. (2016). Flexural behavior of RC beams strengthened by NSM GFRP Bars having different end conditions, Composite Structures, 147, pp. 131-142.

[9] Sharaky, I.A., Torres, L. and Sallam, H.E.M. (2015). Experimental and analytical investigation into the flexural performance of RC beams with partially and fully bonded NSM FRP bars/strips, Composite Structure, 122, pp. 113-126.

[10] Sallam, H.E.M., Saba, A.M., Shaheen, H.H. and Abdel-Raouf, H. (2004). Prevention of peeling failure in plated beams, J Adv Concr Technolo, JCI, 2(3), pp. 419-429.

[11] Sharaky, I.A., Torres, L., Comas, J. and Barris, C. (2014). Flexural response of reinforced concrete (RC) beams strengthened with near surface mounted (NSM) fibre reinforced polymer (FRP) bars, Composite Structures, 109, pp. 8-22.

[12] Parretti, R. and Nanni, A. (2004). Strengthening of RC members using near-surface mounted FRP composites: design overview, Advances in Structural Engineering, 7(6), pp. 469-483.

[13] Hassan, T. and Rizkalla, S. (2004). Bond mechanism of near surface mounted fibre reinforced polymer bars for flexural strengthening of concrete structures, ACI Structure Journal, 101(6), pp. 830-839.

[14] Al Mahmoud, F., Castel, A., François, R. and Tourneur, C. (2009). Strengthening of RC members with near-surface mounted CFRP rods, Composite Structure, 91(2), pp. 138-147.
[15] Pereira, S. S. R., Carvalho, H., Dias, J. V. F., Verga M, V. R. and Montenegro, P. A. (2019). Behaviour of precast reinforced concrete columns subjected to monotonic short-term loading. Frattura ed Integrita Strutturale, 13(50), 242-250. DOI: 10.3221/IGF-ESIS.50.20.
[16] Dias, J. V. F., Oliveira, J. P. S., Calenzani, A. F. G. and Fakury, R. H. (2019). Elastic critical moment of lateral-distortional buckling of steel-concrete composite beams under uniform hogging moment. International Journal of Structural Stability and Dynamics, 19(7). DOI: 10.1142/S0219455419500791.
[17] Santos, L. R. D., Cardoso, H. D. S., Caldas, R. B. and Grilo, L. F. (2020). Finite element model for bolted shear connectors in concrete-filled steel tubular columns. Engineering Structures, 203. doi:10.1016/j.engstruct.2019.109863.
[18] Hawileh, R.A. (2012). Nonlinear finite element modeling of RC beams strengthened with NSM FRP rods, Construction and Building Materials, 27, pp. 461-471.
[19] EL-Emam, H., El-Sisi, A., Reda, R.M., Seleem, M.H. and Bneni, M. (2020). Effect of concrete cover thickness and main reinforcement ratio on flexural behavior of RC beams strengthened by NSM-GFRP bars, Frattura ed Integrità Strutturale, 52, pp.197–210. DOI: 10.3221/IGF-ESIS.52.16.
[20] Sharaky, I.A., Selmy, S.A.I., El-Attar and M.M., Sallam, H.E.M. (2020). The influence of interaction between NSM and internal reinforcements on the structural behavior of upgrading RC beams, Composite Structures, 234-111751.
[21] ANSYS, Inc. (2018). Release 19.0 Documentation for Ansys.
[22] Hawileh, R.A., Rahman, A. and Tabatabai, H. (2010). Nonlinear finite element analysis and modeling of a precast hybrid beam–column connection subjected to cyclic loads, Applied Mathematical Modelling, 34, pp. 2562-2583.
[23] Yan, F. and Lin, Z. (2016). Bond behavior of GFRP bar-concrete interface: damage evolution assessment and FE simulation implementations, Composite Structures, 155, pp. 63-76.
[24] Sharaky, I.A., Reda, R.M., Ghanem, M., Seleem, M.H. and Sallam, H.E.M. (2017). Experimental and numerical study of RC beams strengthened with bottom and side NSM GFRP bars having different end conditions, Construction and Building Materials, 149, pp. 882-903.
[25] Shabana, I.S., Sharaky, I.A., Khalil, A., Hadad, H.S. and Arafa, E.M. (2018). Flexural response analysis of passive and active near surface- mounted joints: experimental and finite element analysis, Materials and Structures, 51(107), pp. 1-15.
[26] Omran, H.Y. and El-Hacha, R. (2012). Nonlinear 3D finite element modeling of RC beams strengthened with prestressed NSM-CFRP strips, Construction and Building Materials, 31, pp. 74-85.
[27] CEB-FIP Model Code 1990. Design code; (1993).